

† chaoliu@slac.stanford.edu

klystron forward (FWD), which is directly after the klystron, and the cavity forward (FWD) and cavity reflection (REF) just before the structure as shown in 2. The peak power delivered to the structure ranges from around 4 MW to 16.45 MW for this experiment. The measurement results used in this paper are captured at two peak power levels, 5.17 and 16.45 MW. To avoid damage to the structure, the 5.17 MW peak power is used to operate the system with longer pulses at lower power, and the 16.45 MW peak power is used to operate the system with a shorter pulse and higher power. A more detailed description of the test stand is available in [4].

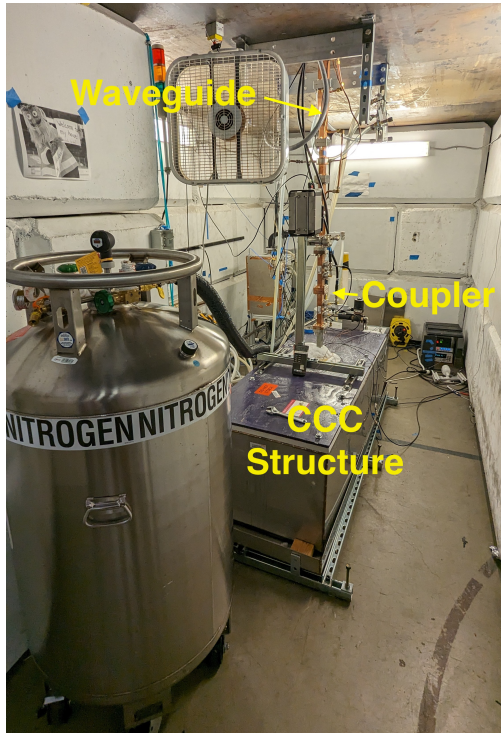


Figure 2: The high-power RF pulse with different shapes injected to a prototype C³ structure.

PULSE MODULATION SCHEMES

This test aims to demonstrate the high-precision RF pulse generation and measurement capability of NG-LLRF. In this experiment, the test stand was driven by RF pulses modulated with three different schemes, the square pulse, the pulse train, and the pulse with phase reversal, at 10 Hz, with a pulse width of 1 μ s, and the peak power of 5.17 MW. The same test procedure was used for all test cases. In software, the baseband waveform is loaded to the BRAM in the FPGA and then the data is accessed by the firmware. The data is interpolated and up mixed with a numerical controlled oscillator around 5.712 GHz by a digital up converter (DUC) in RFSoc. The up-converted samples are streamed to a DAC, which generates the RF pulse. The RF signals from the couplers are attenuated and then captured by the integrated ADCs in the RFSoc. The ADCs samples are down mixed and decimated by a digital down converter (DDC) in RFSoc.

The base-band data is recorded in in-phase (I) and quadrature (Q) format. The IQ samples are converted to magnitude and phase for further analysis in this case.

Square RF pulse

The square RF pulse is the most common waveform used to drive the accelerating structures. Figure 3 shows the base-band pulses captured at different stages when the test stand was driven by square RF pulses. The pulses measured with the square pulse drive are used as references for analyzing the pulses measured with other pulse shapes. The magnitude of the klystron forward signal reached a flat top in around 0.3 μ s and the flat top is approximately 0.7 μ s in this case. The magnitude of the cavity forward signal shows a similar trend with the klystron forward, but with a slight decrease until the RF is off, which can be attributed to cross-coupling with the cavity reflection as observed in [4]. The magnitude of the cavity reflection decreases linearly with time as the field fills the cavity. The cavity is fully filled in about 0.75 μ s, when the magnitude of the reflection signal reaches zero. The RF power afterwards is fully reflected as the magnitude increases and the phase reverses. When the RF is switched off, there is a sharp rise in the reflection signal, since there is no beam in this case, and the structure was designed to be critically coupled to the beam. Then the magnitude of reflection decays as the field energy dissipates in the structure.

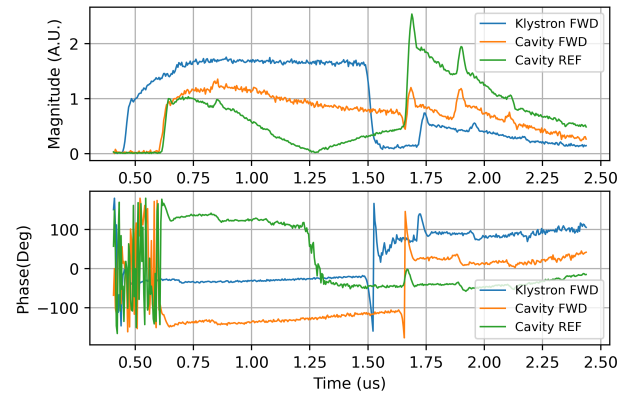


Figure 3: The magnitude and phase of the base-band pulses measured with a 1 μ s square RF pulse at the peak power of 5.17 MW.

Pulse Train

Figure 4 shows the base-band pulses captured at different stages when the test stand was driven by pulses with RF switch on and off every 0.2 μ s. As the klystron forward and cavity forward signals show, the desired pulse shape has been produced. The magnitude of the reflection signal declines when the RF is on, but does not reach zero within the pulse, which means that the structure has not been filled.

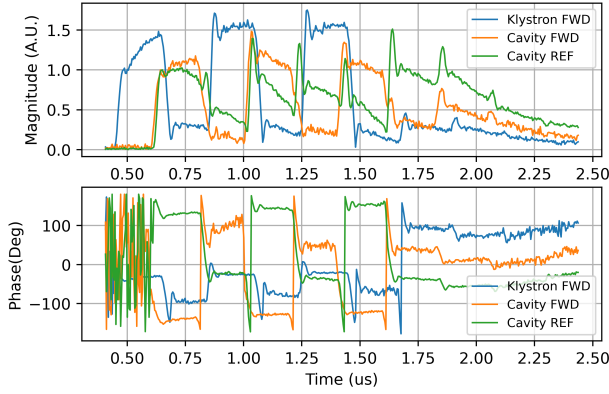


Figure 4: The magnitude and phase of the base-band pulses measured with a $1 \mu\text{s}$ pulse with RF switch on and off every $0.2 \mu\text{s}$ at the peak power of 5.17 MW.

Pulse with Phase Reversal

Figure 5 shows the base-band pulses captured at different stages when the test stand was driven by pulses with RF phase reversal every $0.2 \mu\text{s}$. The klystron forward and cavity forward signals show that the phase reversals have been successfully introduced. The magnitude and phase of the reflection signal demonstrate that the field energy is extracted when the phase of the drive signal is reversed, and then the RF with the reversed phase starts filling the structure. This cycle repeats until the RF is switched off, and then the reflection signal delays as the energy dissipates in the structure.

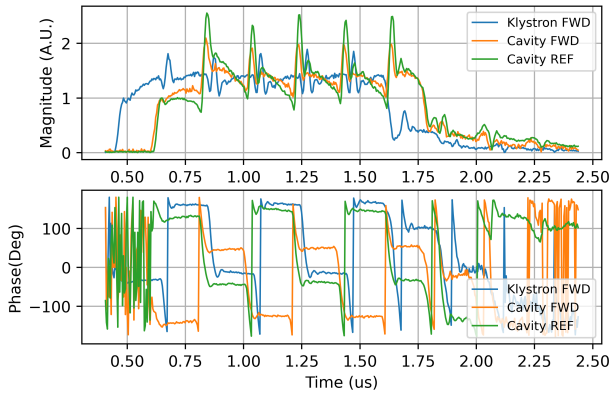


Figure 5: The magnitude and phase of the base-band pulses measured with a $1 \mu\text{s}$ pulse with RF phase reversal every $0.2 \mu\text{s}$ at the peak power of 5.17 MW.

Pulse with Linear Phase Ramp

Figure 6 shows the base-band pulses captured at different stages when the test stand was driven by pulses with a linear phase ramp. The klystron forward and cavity forward signals show that the phase ramp has been successfully introduced. However, the RF power injected into the structure is fully reflected, as the phase ramp is equivalent to drive the structure off resonance.

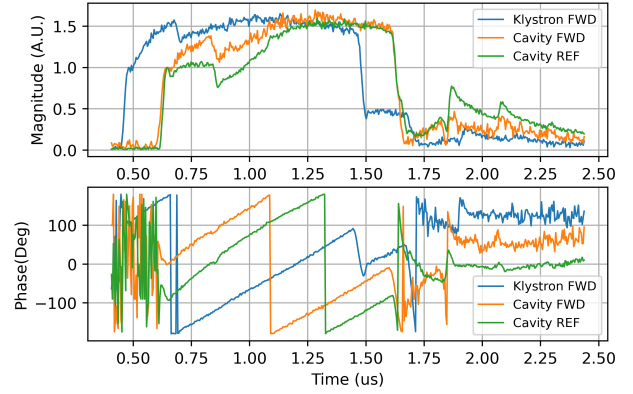


Figure 6: The magnitude and phase of the base-band pulses measured with a $1 \mu\text{s}$ pulse with a 360° linear phase ramp at the peak power of 5.17 MW.

PHASE REVERSAL FOR SLED

The phase reversal test has also been performed with a $0.45 \mu\text{s}$ RF pulse with a peak power of 16.45 MW. The klystron forward and cavity forward signal in Figure 7 show that phase reversal has been introduced precisely. The reflection pulse shows that the field fills the structure for the initial $0.2 \mu\text{s}$. When the phase of RF drive is reversed, the magnitude of the reflection signal increased to more than twice the initial peak, and the phase reverses. Rapid power extraction demonstrated the technique required by the SLED.

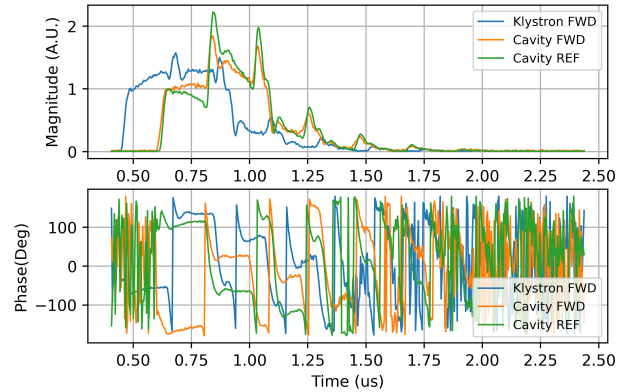


Figure 7: The magnitude and phase of the base-band pulses measured with a $0.45 \mu\text{s}$ pulse with phase reversal every $0.2 \mu\text{s}$ at the peak power of 16.45 MW.

SUMMARY

Direct RF sampling with integrated data converters in RFSoc demonstrated flexibility in generating and measuring arbitrary pulse shapes with the C-band high-power test stand and the prototype C³ structure. The NG-LLRF system successfully demonstrated the rapid power extraction required by SLED. The duration and relative timing of the phase reversal can be tuned to control a real SLED structure.

REFERENCES

- [1] Z. Farkas *et al.*, “Sled: A method of doubling slac’s energy”, *Proc. Of 9th Int. Conf. On High Energy Accelerators, SLAC*, p. 576, 1974.
- [2] S. Kashiwagi *et al.*, “Beam loading compensation using phase to amplitude modulation method in atf”, *roceedings of the XIX International Linear Accelerator Conference*, p. 91-93, 1998.
- [3] C. Liu *et al.*, “Next Generation LLRF Control Platform for Compact C-band Linear Accelerator”, *LCWS2024, EPJ Web of Conferences*, vol. 315, no. 4, p. 02008, 2024. doi:10.1051/epjconf/202431502008
- [4] C. Liu *et al.*, “High-power test of a C-band linear accelerating structure with an RFSoc-based LLRF system”, *Review of Scientific Instruments*, vol. 96, no. 4, 2025. doi:10.1063/5.0258520
- [5] E. Nanni *et al.*, “ESPPU INPUT: C3 within the "Linear Collider Vision" ”, *arXiv preprint arXiv:2503.20829*, 2025. <https://arxiv.org/abs/2503.20829>
- [6] C. Liu *et al.*, “Characterizing the performance of high-speed data converters for RFSoc-based radio astronomy receivers”, *Monthly Notices of the Royal Astronomical Society*, vol. 501, no. 4, p. 5096–5104, 2021. doi:10.1093/mnras/staa3895
- [7] C. Liu *et al.*, “Development of General-purpose Digital Backend for Single-dish Centimetre and Millimetre-wave Telescopes”, *3rd URSI Atlantic and Asia Pacific Radio Science Meeting (AT-AP-RASC)*, 2022. doi:10.23919/AT-AP-RASC54737.2022.9814190
- [8] S. Henderson, C. Liu *et al.*, “Advanced RFSoc readout for space-based superconducting sensor arrays”, *Millimeter, Sub-millimeter, and Far-Infrared Detectors and Instrumentation for Astronomy XI*, vol. 12190, p. 339-355, 2022. doi:10.1117/12.2630412
- [9] C. Liu *et al.*, “Evaluating Direct RF Sampling Performance for RFSoc-based Radio-frequency Astronomy Receivers”, *XXXVth General Assembly and Scientific Symposium of the International Union of Radio Science (URSI GASS)*, 2023. arXivpreprintarXiv:2309.08067
- [10] C. Liu *et al.*, “Higher order nyquist zone sampling with rf-soc data converters for astronomical and high energy physics readout systems”, *2023 IEEE Nuclear Science Symposium and Medical Imaging Conference*, arXivpreprintarXiv:2309.08640
- [11] C. Liu *et al.*, “Development of RFSoc-based direct sampling highly multiplexed microwave SQUID readout for future CMB and submillimeter surveys”, *2024 SPIE Astronomical Telescopes + Instrumentation*, doi:10.1117/12.3019317
- [12] C. Liu *et al.*, “Direct rf sampling based LLRF control system for C-band linear accelerator”, *IPAC’24 - 15th International Particle Accelerator Conference*, p. 25-28, 2024. doi:10.18429/JACoW-IPAC2024-MOCN2
- [13] C. Liu *et al.*, “A Compact Low-level RF Control System for Advanced Concept Compact Electron Linear Accelerator”, *Submitted to Review of Scientific Instruments*, 2025 <https://arxiv.org/abs/2502.10623>